Modulation contrast optimization for wavelength conversion of a 20 Gbit/s data signal in hybrid InP/SOI photonic crystal nanocavity

Kevin Lenglé, Thanh Nam Nguyen, Mathilde Gay, Laurent Bramerie, Jean-Claude Simon, Alexandre Bazin, Fabrice Raineri, Rama Raj

Modulation contrast optimization for wavelength conversion of a 20 Gbit/s data signal in hybrid InP/SOI photonic crystal nanocavity

K. Lengle[1,2,*], T.N. Nguyen[1,2], M. Gay[1,2], L. Bramerie[1,2], JC. Simon[1,2], A. Bazin[3], F. Raineri[3] and R. Raj[3]

[1] *Université Européenne de Bretagne (UEB), 5 Boulevard Laënnec, 35000 Rennes, France*
[2] *CNRS-Foton Laboratory (UMR 6082), Enssat, CS 80518, 22305 Lannion, France*
[3] *Laboratoire de Photonique et de Nanostructures, CNRS-UPR20, Route de Nozay, 91460 Marcoussis, France*
[*] *Corresponding author: kevin.lengle@enssat.fr*

Compiled March 13, 2014

Photonic crystal cavity-based switching is studied both theoretically and experimentally in order to identify the best configuration to maximize "wavelength conversion" efficiency. In particular, it is shown that an enhanced contrast can be reached when the probe is blue-shifted with respect to the resonance. The use of an InP/SOI hybrid photonic crystal nanocavity is reported for the first time for all-optical error-free "wavelength conversion" at 20 Gbit/s with an NRZ-OOK signal.

OCIS codes: (230.5298) Photonic crystals, (130.4815) Optical switching devices

InP over silicon-on-insulator (SOI) hybrid technology is an extremely promising solution for future photonic circuits as it combines CMOS compatibility with the optoelectronic properties of III-V materials. This hybrid technology has allowed the demonstration of lasers [1], amplifiers [2] and optical flip-flops [3]. The fabrication of microdisks has recently enabled new functions such as wavelength [4] and modulation format [5] conversion to be demonstrated. Meanwhile, photonic crystals (PhCs) are considered to be promising building blocks for high-density photonic integrated circuits. PhC cavities have shown their capacity to provide both small size and high nonlinear response with few fJ activation energies, and are also excellent at achieving optical bistability with low input powers [6, 7]. All-optical switching has been recently demonstrated using an InP over SOI PhC nanocavity and the integration of a PhC nanolaser on top of SOI waveguides confirmed the potential of this hybrid technology for the fabrication of nanophotonic components [8]. However, very few high bit rate system demonstrations have been reported so far, due to the slow response time of fabricated devices. In this work, the common function in the telecommunication field of "wavelength conversion" is realised, which consists in copying the information carried on the "signal wavelength" onto a "probe wavelength". One of the main issues in such a function is to find the best configuration to maximize the contrast of the converted signal. In this letter, we address this issue by studying the switching properties, in particular the modulation contrast, thanks to simulations based on coupled mode theory in InP-based PhC nanocavity integrated on SOI waveguide. Afterwards, an experimental assessment in such hybrid device is reported, confirming the predicted contrast behaviour. Finally, "wavelength conversion" is demonstrated for the first time in a system experiment at 20 Gbit/s using a PhC nanocavity based on III-V/SOI hybrid technology, which incorporates an active material optimized for ultrafast operation.

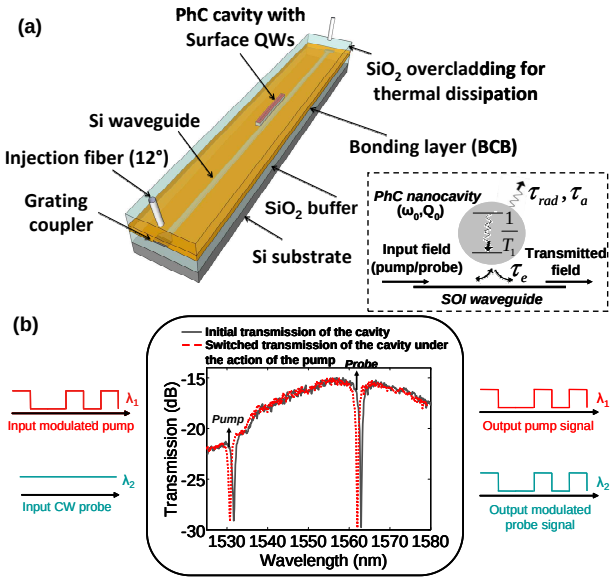

Figure 1. (a) Schematic representation of the device (inset : modeled system). (b) "Wavelength conversion" principle with normalized transmission spectrum.

The device is represented in Fig. 1(a). It is composed of two optical levels. The first level is a single mode SOI wire waveguide. The second one is an InP-based PhC nanocavity. The studied nanocavity is a nanobeam cavity [9], which is formed by drilling equally sized holes in a single mode InP wire waveguide (600 nm × 260 nm × 15 μm). The design of the cavity is based on the use of Gaussian apodization of the electromagnetic field profile within the cavity [10], by fine-tuning the distance between holes. The cavity is fully encapsulated in silica (SiO_2) in order to improve heat sinking, which is important in the context of high

speed operation. More details on this cavity can be found in [11]. The transmission spectrum is plotted in Fig. 1(b), presenting two resonant modes at 1532nm et 1563nm. As shown in Fig. 1(a), grating couplers are etched at each extremity of the SOI waveguide to allow coupling with cleaved-facet single-mode optical fibers with reduced coupling loss [12]. Optimal coupling is obtained for a fiber angle of 12° at a working wavelength of 1560 nm (25% coupling efficiency).

A judicious combination of the manipulation of the carrier lifetime in InP-based materials through surface growth of quantum wells (QWs) and material processing so as to maximise the speed of the nonlinear response was also carried out in the present device, as described in [11], with the view to obtaining high speed all optical switches. The principle of operation of our wavelength converter is schematically represented in Fig. 1(b). The optical pumping of the III-V semiconductor active material by the incident signal power induces a change in the carrier density. This leads to a dynamic change in the refractive index and hence a shift in the resonance wavelengths of the cavity. This is the well known blue-shift. A continuous-wave probe signal is set around the other resonance which has the effect of transferring information contained in the control signal (pump) to the cw probe signal as it modifies the transmission experienced by this signal. The extinction ratio of the modulated probe corresponds to the modulation contrast subsequently used.

The modeled device is presented in this section. Coupling by evanescent waves occurs when a waveguide and a cavity are at distances close enough so that spatial overlap of their modes is achieved. The coupled mode theory (CMT) is well suited to address this problem [13]. Structures such as microdisks or photonic crystals cavities have been modeled in this way. The modeled system is schematically represented in the inset of Fig. 1, where τ_{rad} is the cavity lifetime limited by the radiative losses, τ_e is related to the cavity coupling, τ_a is related to the material absorption and T_1 is the population lifetime. The model considered here is that of a single mode cavity (resonance at ω_0 and quality factor of the cold cavity Q_0) coupled to a waveguide. The overall photon lifetime τ in the cavity is given by

$$\frac{1}{\tau} = \frac{2}{\tau_e} + \frac{1}{\tau_{rad}} + \frac{1}{\tau_a}. \qquad (1)$$

The cavity mode is coupled via the waveguide with the input field f (pump or probe signal), and only the transmited field is considered. The mode amplitude in the cavity $a(t)$ is described by a simple harmonic oscillator model [13]

$$\frac{\partial a}{\partial t} = \left[j(\omega_0 + \Delta\omega) - \frac{1}{\tau} \right] a(t) + \sqrt{\frac{2}{\tau_e}} f(t). \qquad (2)$$

Note that, thermal effects that imply only a well known red-shift of the resonance and not a distortion are not taken into account. We experimentally follow the red-shift by shifting also the probe signal wavelength in order to maximize "wavelength conversion" efficiency. The free carrier density $N(t)$ is described by

$$\frac{\partial N}{\partial t} = \frac{-N(t)}{T_1} - \frac{|a(t)|^2}{T_1 |a_{sat}(t)|^2} [N(t) - N_t], \qquad (3)$$

where $|a_{sat}|^2$ is the saturation power and N_t the carrier density at transparency. The index variations due to the photocreated carriers induce a resonance blue-shift $\Delta\omega$ of the cavity defined by the following equation with τ_{a_0} related to unsaturated absorption

$$\Delta\omega = \frac{\alpha_H}{\tau_{a_0}} \left(\frac{N}{N_t} - 1 \right). \qquad (4)$$

For each lifetime τ_i, a quality factor can be defined by $Q_i = \omega_0 \tau_i / 2$. The parameters chosen for the simulations are Q_{rad}= 5530, defined by radiative losses, Q_{a_0}= 5000, related to unsaturated absorption for small signal, and Q_e= 728, defined by the width of the waveguide, giving a quality factor of the cold cavity Q_0 of 570. Note that, we chose to work with relatively low values of Q in order not to be limited by the photon lifetime in the cavity-based switch. The carrier lifetime is of the order of 30 ps, entirely determined by the non radiative recombination processes [11]. The Henry factor α_H is of the order of 4, since the absorption band of the quantum wells is very close to the working wavelength.

This model is used to simulate a co-propagative pump-probe configuration and calculate the contrast evolution as a function of the detuning of the probe wavelength compared to the center wavelength of the cavity resonance, for several pump powers, as shown in Fig. 2. The model takes into account cross effects of pump and probe signals. As in the following experiment, the probe power is more than hundred times smaller than the pump one and we consider that it does not create modification on the resonances. The pump signal consists of 100 ps Gaussian pulses at a repetition rate of 500 MHz. The polarity of the modulated signal can be inverted or kept unchanged compared to the pump, depending on the probe position relatively to the resonance. Moreover, the higher the pump power, the higher the maximum contrast, as a consequence of the higher resonance shift. A maximum negative contrast of -11 dB is achieved. On the other hand, with the same pump power, only 7 dB of positive contrast is reached, pointing to contrast asymmetry. Note that, these values are very close to the maximum contrast values, as shown in the inset of Fig. 2, which shows the positive and negative contrast maxima as a function of pump power. This asymmetry of the modulation contrast evolution may come from a distortion of the resonance when it dynamically shifts under the influence of the pump signal, as it will be reported later in the letter. Next, this behaviour was experimentally investigated.

The experimental setup is presented in Fig. 3. The pump signal consists in 100 ps pulses obtained from a

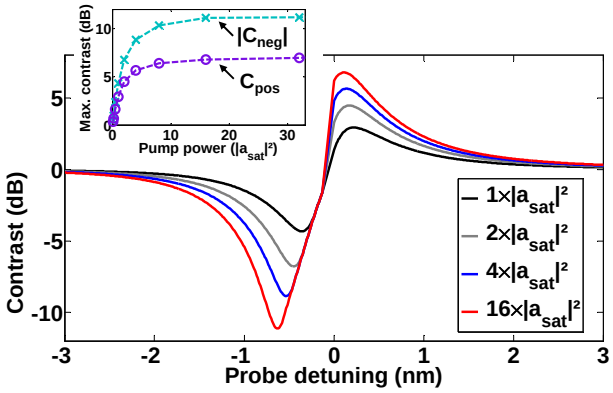

Figure 2. Simulated evolution of the contrast as a function of probe wavelength for different pump powers. Inset: simulated evolution of positive and negative contrast maxima as a function of pump power.

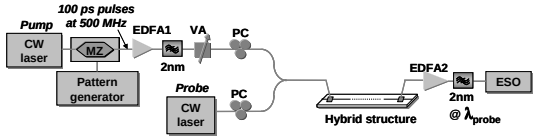

Figure 3. Experimental setup for switching characterization.

continuous laser at 1532 nm, modulated in an external modulator with a 10 Gbit/s pattern generator. The repetition rate of 500 MHz is obtained by programming the pattern generator to reach a high peak-to-average power ratio (×20). After being amplified by an erbium doped fiber amplifier (EDFA1) and bandpass filtered to limit the noise bandwidth, the pump signal is combined with the continuous-wave tunable probe signal via a 3 dB coupler. The polarization states of the pump and probe are controlled at the input of the device via two separate polarization controllers (PCs) to align them with the TE mode of the device. At the output of the device, the probe signal is amplified (EDFA2), and then filtered to limit the noise bandwidth before reaching an electrical sampling oscilloscope (ESO) (50 GHz bandwidth). To obtain an output modulated probe signal, the probe wavelength was set around the long wavelength cavity resonance. The reason to choose the longer wavelength resonance for the probe signal is that it has a higher static extinction ratio as compared to that of the shorter resonance wavelength and will give an intrinsic higher extinction ratio in the output.

Figure 4 presents the results of contrast as a function of probe wavelength for different coupled pump powers. The contrast curves experience a slight red-shift as the pump power is increased due to thermal effects induced by pump heating. The behaviour predicted in the numerical simulations, namely an asymmetry between positive and negative contrast maxima, is confirmed regardless of pump power. Indeed, for a coupled pump power of 0 dBm, a maximum positive contrast around

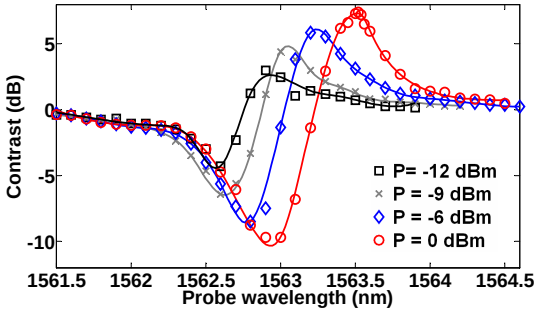

Figure 4. Measured modulation contrast as a function of probe wavelength for different coupled pump powers. The symbols represent measured data while the lines are cubic spline fits.

7 dB is measured, whereas the maximum negative contrast is around -10 dB for the same pump power.

Based on the CMT model, the value of the probe signal transmission at the instant corresponding to the maximum of the pump pulse is found using numerical simulations for each wavelength position of the probe signal. At this point, the carrier density is the highest and, therefore, the shift of the resonance is the largest. It is then possible to deduce the profile of the dynamic shifted resonance, as shown in Fig. 5. It can be seen that the shifted resonance is deeper compared to the initial static resonance. This reconstructed shifted resonance gives a better understanding of why the negative contrast is larger than the positive contrast, symbolized by $-$ and $+$ in Fig. 5. By subtracting both resonance profiles (inset of Fig. 5), the asymmetric shape of the contrast evolution previously obtained is retrieved. The modeling carried out using the CMT allows to demonstrate a decreased absorption during injection of the pump signal (which implies an increase of τ_a). From Eq. 1, this results in an increase in the overall photon lifetime in the cavity, causing an increase in the quality factor of the dynamic cavity. This is the origin of the maxima asymmetry between positive and negative contrasts observed experimentally and in the modeling results. It is therefore advisable to exploite negative contrast to maximize the modulation contrast in practical applications.

Thereafter "wavelength conversion" was performed at 20 Gbit/s. The experimental setup is similar to the one in Fig. 3, except that the pump signal is now a 20 Gbit/s non-return to zero on-off keying (NRZ-OOK) signal modulated with a $2^7 - 1$ pseudo random binary sequence (PRBS). The pump signal is at 1532 nm and the probe signal is tuned to 1563 nm, i.e. slightly below the resonance as thermal effects slightly red-shift the resonances under the pump power action. This configuration inverts the polarity of the signal (negative contrast) to take advantage of the previously demonstrated results. The average coupled pump power is estimated to be 3 dBm, which corresponds to a

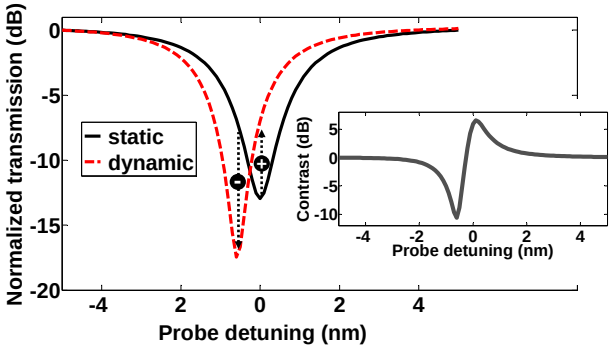

Figure 5. Initial static resonance (black line) and shifted resonance reconstructed thanks to CMT (red dotted line) for a pump power of $16 \times |a_{sat}|^2$. + and − symbols represent the maximum positive and negative contrasts possibly achieved. Inset : evolution of the contrast obtained by subtracting both resonance profiles.

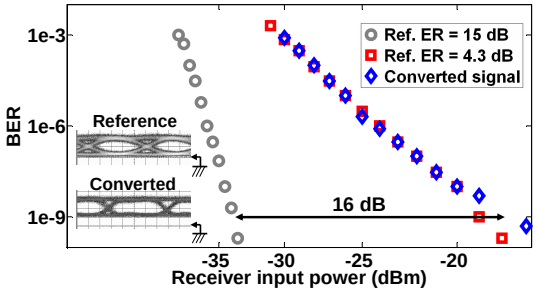

Figure 6. BER as a function of the receiver input power for "wavelength conversion" at 20 Gbit/s. Inset: Eye diagrams of reference and converted signals.

cavity switching energy of 200 fJ. The optical bistability is not reached for the power levels and position of the pump signal used in this study. With this power, a limited contrast of 4.3 dB is measured, which can not be increased further because of the power damage threshold of the device. This value is below the maximum contrast reached in the previous characterisation as the peak-to-average power ratio is much lower. The bit error rate (BER) is measured as a function of the receiver input power in the back-to-back case (transmitter directly in front of the receiver) and for the wavelength converted signal. Error-free operation is achieved, but with 16 dB power penalty at a BER of 10^{-9}, despite a good opening of the eye diagram, as shown in the inset of Fig. 6. In order to evaluate the origin of this penalty, the BER is measured in the back-to-back configuration using a signal with an artificially degraded extinction ratio equal to the converted signal extinction ratio. The resulting BER curve is plotted with red squares in Fig. 6, showing a good agreement with the wavelength converted curve. It can thus be concluded that the low extinction ratio of the wavelength converted signal is at the origin of the BER degradation, and that the time response of the component has no impact on the BER at this bit rate.

In conclusion, fast switching was reported in a system experiment using a hybrid InP-based PhC nanocavity integrated on a SOI waveguide. The modulation contrast behaviour was studied thanks to coupled mode theory. This study shows that the negative modulation contrast allows to maximize the modulation efficiency in "wavelength conversion" due to the narrowing of the dynamic resonance shape. With the very good switching characteristics measured dynamically, the device was used for NRZ-OOK "wavelength conversion" at 20 Gbit/s with error-free operation without limitation by its time response. Our results confirm the huge potential of nanophotonic III-V/SOI technologies for all-optical signal processing in very small footprints and low energy consuming components.

We acknowledge helpful discussions with Y. Dumeige and support by the EU through the Copernicus project (249012).

References

1. J. Van Campenhout, P. Romeo, P. Regreny, C. Seassal, D. Van Thourhout, L. Di Cioccio, JM. Fedeli, and R. Baets, Opt. Express **15**, 6744 (2007).
2. H. Park, A. Fang, O. Cohen, R. Jones, M. Paniccia, J. Bowers, IEEE Photon. Technol. Lett. **19**, 230 (2007).
3. D.Van Thourhout, T. Spuesens, S. Selvaraja, L. Liu, G. Roelkens, R. Kumar, G. Morthier, P. Rojo-Romeo, F. Mandorlo, P. Regreny, O. Raz, C. Kopp, L. Grenouillet, IEEE J. Sel. Topics Quantum Electron. **16**, 1363, (2010).
4. R. Kumar, T. Spuesens, P. Mechet, P. Kumar, O. Raz, N. Olivier, J. Fedeli, G. Roelkens, R. Baets, D. Van Thourhout, G. Morthier, Opt. Lett. **36**, 2450 (2011).
5. R. Kumar, T. Spuesens, P. Mechet, N. Olivier, J. Fedeli, P. Regreny, G. Roelkens, D. Van Thourhout, G. Morthier, Opt. Exp. **19**, 24647 (2011).
6. A. Yacomotti, F. Raineri, G. Vecchi, P. Monnier, R. Raj, A. Levenson, B. Ben Bakir, C. Seassal, X. Letartre, P. Viktorovitch, L. Di Cioccio, J.M. Fedeli, Appl. Phys. Lett. **88**, 231107 (2006).
7. K. Nozaki, A. Shinya, S. Matsuo, Y. Suzaki, T. Segawa, T. Sato, Y. Kawaguchi, R. Takahashi, M. Notomi, Nature **6**, 248 (2012)
8. Y. Halioua, A. Bazin, P. Monnier, T. Karle, G. Roelkens, I. Sagnes, R. Raj, F. Raineri, Opt. Express **19**, 9221 (2011).
9. J. Foresi, P. Villeneuve, J. Ferrera, E. Thoen, G. Steinmeyer, S. Fan, J. Joannopoulos, L. Kimerling, H. Smith, E. Ippen, Nature **390**, 143 (1997).
10. Y. Tanaka, T. Asano, S. Noda, IEEE J. Lightw. Technol. **26**, 11, 1532 (2008).
11. A. Bazin, K. Lengle, M. Gay, P. Monnier, L. Bramerie, R. Braive, G. Beaudoin, I. Sagnes, R. Raj, F. Raineri, Appl. Phys. Lett. **104**, 011102 (2014).
12. D. Taillaert, F. Van Laere, M. Ayre, W. Bogaerts, D. Van Thourhout, P. Bienstman, R. Baets, Jpn. J. Appl. Phys. **45**, 8A, 6071 (2006).
13. H.A. Haus, "Waves and Fields in Optoelectronics", Prentice-Hall Inc. (1984).

Informational Fourth Page

References

1. J. Van Campenhout, P. Romeo, P. Regreny, C. Seassal, D. Van Thourhout, L. Di Cioccio, JM. Fedeli, R. Baets, "Electrically pumped InP-based microdisk lasers integrated with a nanophotonic silicon-on-insulator waveguide circuit", Opt. Express **15**, 6744-6749 (2007).
2. H. Park, A. Fang, O. Cohen, R. Jones, M. Paniccia, J. Bowers, " A hybrid AlGaInAs–silicon evanescent amplifier", IEEE Photon. Technol. Lett., **19**, 230-232 (2007).
3. D.Van Thourhout, T. Spuesens, S. Selvaraja, L. Liu, G. Roelkens, R. Kumar, G. Morthier, P. Rojo-Romeo, F. Mandorlo, P. Regreny, O. Raz, C. Kopp, L. Grenouillet, "Nanophotonic devices for Optical Interconnect", IEEE J. Sel. Topics Quantum Electron. **16**, p. 1363-1375, (2010).
4. R. Kumar, T. Spuesens, P. Mechet, P. Kumar, O. Raz, N. Olivier, J. Fedeli, G. Roelkens, R. Baets, D. Van Thourhout, G. Morthier, "Ultrafast and bias-free all-optical wavelength conversion using III-V-on-silicon technology," Opt. Lett. **36** (13), p. 2450-2452 (2011).
5. R. Kumar, T. Spuesens, P. Mechet, N. Olivier, J. Fedeli, P. Regreny, G. Roelkens, D. Van Thourhout, G. Morthier, "10Gbit/s all-optical NRZ-OOK to RZ-OOK format conversion in an ultra-small III-V-on-silicon microdisk fabricated in a CMOS pilot line", Opt. Exp. **19** (24),p. 24647 (2011).
6. A. Yacomotti, F. Raineri, G. Vecchi, P. Monnier, R. Raj, A. Levenson, B. Ben Bakir, C. Seassal, X. Letartre, P. Viktorovitch, L. Di Cioccio, J.M. Fedeli, "All-optical bistable band-edge Bloch modes in a two-dimensional photonic crystal", Appl. Phys. Lett. **88**, 231107-231107 (2006).
7. K. Nozaki, A. Shinya, S. Matsuo, Y. Suzaki, T. Segawa, T. Sato, Y. Kawaguchi, R. Takahashi, M. Notomi, "Ultralow-power all-optical RAM based on nanocavities", Nature Photonics, Nature **6**, 248-252 (2012)
8. Y. Halioua, A. Bazin, P. Monnier, T. Karle, G. Roelkens, I. Sagnes, R. Raj, F. Raineri, "Hybrid III-V semiconductor/silicon nanolaser", Opt. Express **19** (10), 9221-9231 (2011).
9. J. Foresi, P. Villeneuve, J. Ferrera, E. Thoen, G. Steinmeyer, S. Fan, J. Joannopoulos, L. Kimerling, H. Smith, E. Ippen, "Photonic-bandgap microcavities in optical waveguides", Nature **390** (6656), 143-145 (1997).
10. Y. Tanaka, T. Asano, S. Noda, "Design of Photonic Crystal Nanocavity With Q-Factor of 10^9" J. Lightw. Technol., **26** (11), 1532-1539 (2008).
11. A. Bazin, K. Lengle, M. Gay, P. Monnier, L. Bramerie, R. Braive, G. Beaudoin, I. Sagnes, R. Raj, F. Raineri, "Ultrafast all-optical switching and error-free 10 Gbit/s wavelength conversion in hybrid InP-silicon on insulator nanocavities using surface quantum wells", Appl. Phys. Lett. **104**, 011102 (2014)
12. D. Taillaert, F. Van Laere, M. Ayre, W. Bogaerts, D. Van Thourhout, P. Bienstman, R. Baets, "Grating couplers for coupling between optical fibers and nanophotonic waveguides", Jpn. J. Appl. Phys. **45** (No. 8A), 6071-6077 (2006).
13. H.A. Haus, "Waves and Fields in Optoelectronics", Prentice-Hall Inc. (1984).